ELSEVIER

Tectonophysics 322 (2000) 19–33

TECTONOPHYSICS

www.elsevier.com/locate/tecto

Early formation and long-term stability of continents resulting from decompression melting in a convecting mantle

J. De Smet *, A.P. Van den Berg, N.J. Vlaar

Department of Theoretical Geophysics, University of Utrecht, P.O. Box 80.021, 3508 TA Utrecht, The Netherlands

Received 19 January 1999; accepted for publication 20 September 1999

Abstract

The origin of stable old continental cratonic roots is still debated. We present numerical modelling results which show rapid initial formation during the Archaean of continental roots of ca. 200 km thick. These results have been obtained from an upper mantle thermal convection model including differentiation by pressure release partial melting of mantle peridotite. The upper mantle model includes time-dependent radiogenic heat production and thermal coupling with a heat reservoir representing the Earth's lower mantle and core. This allows for model experiments including secular cooling on a time-scale comparable to the age of the Earth. The model results show an initial phase of rapid continental root growth of ca. 0.1 billion year, followed by a more gradual increase of continental volume by addition of depleted material produced through hot diapiric, convective upwellings which penetrate the continental root from below. Within ca. 0.6 Ga after the start of the experiment, secular cooling of the mantle brings the average geotherm below the peridotite solidus thereby switching off further continental growth. At this time the thickness of the continental root has grown to ca. 200 km. After 1 Ga of secular cooling small scale thermal instabilities develop at the bottom of the continental root causing continental delamination without breaking up the large scale layering. This delaminated material remixes with the deeper layers. Two more periods, each with a duration of ca. 0.5 Ga and separated by quiescent periods were observed when melting and continental growth was reactivated. Melting ends at 3 Ga. Thereafter secular cooling proceeds and the compositionally buoyant continental root is stabilized further through the increase in mechanical strength induced by the increase of the temperature dependent mantle viscosity. Fluctuating convective velocity amplitudes decrease to below 10 mma^{-1} and the volume average temperature of the sub-continental convecting mantle has decreased ca. 340 K after 4 Ga. Surface heatflow values decrease from 120 to 40 $mW\,m^{-2}$ during the 4 Ga model evolution. The surface heatflow contribution from an almost constant secular cooling rate was estimated to be 6 $mW\,m^{-2}$, in line with recent observational evidence. The modelling results show that the combined effects of compositional buoyancy and strong temperature dependent rheology result in continents which overall remain stable for a duration longer than the age of the Earth. Tracer particles have been used for studying the patterns of mantle differentiation in greater detail. The observed (p, T, F, t)-paths are consistent with proposed stratification and thermo-mechanical history of the depleted continental root, which have been inferred from mantle xenoliths and other upper mantle samples. In addition, the particle tracers have been used to derive the thermal age of the modelled continental root, defined by a hypothetical closing temperature.

Keywords: Archaean; continental roots; continent-formation; mantle convection; pressure-release melting; secular-cooling

* Corresponding author. Present address: Philips Centre for Industrial Technology, P.O. Box 218/SAQ p518, 5600 Eindhoven, The Netherlands.

E-mail addresses: smet@geo.uu.nl (J. De Smet), berg@geo.uu.nl (A. Van den Berg), vlaar@geo.uu.nl (A. Vlaar)

0040-1951/00/$ - see front matter
PII: S0040-1951(00)00055-X

1. Introduction

The oldest continental shields have been stable for several billions of years. The origin of these regions and the reason for their long term stability is still debated. From seismological evidence (Jordan, 1975; LeFevre and Helmberger, 1989; Anderson, 1990; Woodhouse and Trampert, 1995; Polet and Anderson, 1995) and interpretation of the gravity field (Doin et al., 1996), and surface heat flow data (Pollack and Chapman, 1977; Nyblade and Pollack, 1993; Rudnick et al., 1998) for continental regions it has been concluded that continents are underlain by thick roots of compositionally distinct material. Analysis of mantle xenoliths from different continental regions (Jordan, 1979; Griffin et al., 1996) has shown that the continental roots consist of residual material from pressure release partial melting of mantle peridotite.

We have developed a numerical mantle convection model to investigate the formation of continents during the Archaean and their subsequent thermo-mechanical evolution since the late Archaean and Proterozoic.

In previous work (De Smet et al., 1998, 1999) we presented results which focused on the formation and early evolution of the first several hundred million years after the initiation of continental formation. It was shown that, after initiation, continental roots may have grown rapidly be addition from below of depleted peridotite in relatively small scale (± 50 km), hot and melt-producing diapiric upwellings which intermittently penetrate the growing continental root.

Here we present results of numerical modelling which deal with the long term evolution of continents from their formation in the early Earth until the present day. We also present an analysis of detailed temporal and spatial evolution of tracer particles which sample several physical quantities in the diapiric melting process.

Finally we have investigated the evolution of the 'thermal age' of evolving continental roots, defined as the elapsed time since a sample of mantle rock has cooled below a hypothetical closing temperature. The results show a vertical layering in thermal age related to the mechanism of growth from below. This layering is disturbed laterally by thermal rejuvenation by hot diapiric upwellings which overprint existing thermal age during the later evolution.

2. Model description

The model used here is identical to one of the models (Model A) described in more detail by De Smet et al. (1999). Important features of the model are: the use of a melting phase diagram for mantle peridotite with linear solidus and liquidus which practically limits occurrence of partial melting to the upper mantle above the transition zone at ca. 400 km depth. The mantle model is truncated at the upper to lower mantle boundary at a depth of 670 km. Thermal coupling between the upper mantle and the lower mantle and core is important in the thermal evolution models which operate on a time scale of several billion years where secular cooling of the Earth is significant. Therefore, we have extended the upper mantle model with a simple isothermal heat reservoir which accounts for the influence of lower mantle and core on the secular cooling of the upper mantle. We refer to De Smet et al. (1999) for a detailed discussion of the boundary conditions. The applied numerical modelling techniques (De Smet et al., 2000) consist of finite element solutions for the temperature T and the convective velocity field $\boldsymbol{u}$. The degree of depletion F is defined as the mass fraction of melt extracted from the partially melted mantle material. Due to the occurrence of small (km) scale strength the F field is computed on a high resolution (sub-km scale) structured grid. Passive particle tracers are advected with the mantle flow in order to monitor the F, T, pressure p, and thermal age t_{close} for several hypothetical closing temperatures T_{close}.

2.1. Time convention

For elapsed model time we use Ma or Ga where the model evolution starts at $t=0$ Ma. In some discussions b.p. or Ga b.p. is used, meaning the time before present, that is, this is the age of the model measured from a present day situation back

in time. We used for the present day model situation a model evolution time of 4000 Ma, that is, 0 Ma b.p. = 4000 Ma (end of the model computations) and 4000 Ma b.p. = 0 Ma (start of the model computations). See Section 3.4 for the application of this choice.

3. Modelling results

3.1. Model evolution up to 4 billion years

Fig. 1 shows the long-term evolution of the continental upper mantle model. The left-hand-side column shows snapshots of the compositional field from 0.7 to 4.0 Ga. On top of the depleted mantle the lower and upper crustal layers are represented as black and white areas, respectively. At corresponding times the lateral variations in the temperature fields, that is, T–$\langle T\rangle_{\mathrm{hor}}$, are depicted in the right-hand-side column of Fig. 1. The extreme temperature values are not actually attained, which can be seen when the shown temperature variations at 2500 Ma are compared with the actual temperature field as given in Fig. 9 for 1500 Ma b.p. (the vertical scales are not identical for both figures). All frames for both the temperature and composition also contain instantaneous stream-lines of the convective velocity. Black and white lines correspond to clock and counter-clockwise flows, respectively.

Following the evolution in the F-field from 0.7 to 2.5 Ga we see that the total volume of depleted continental root increases. After 2.5 Ga, this increase of the depleted volume has stopped. Mantle differentiation has apparently ceased between 2.5 and 3.0 Ga.

The transition from root to mantle is set at the depth where $F \approx 10\%$. Up to ca. 2.0 Ga the compositional layering is relatively undisturbed and the root extends to depths varying between 150 and 300 km. Hot upwellings are sporadically penetrating the continental root after a model time of ca. 2 Ga. This is related to the increase in the occurrence of delamination of the continental root, which in turn results from the advancing cooling from the top down of the upper mantle system. Hot diapiric upwellings underneath old continental shields do occur at present (e.g., Yellowstone hotspot in North-America) or in the past in Africa (Ebinger and Sleep, 1998). A catastrophical large-scale overturn is, however, not observed during the investigated time-window. Depleted continental root delaminates by relatively small thread-like structures, which sometimes reach the upper to lower mantle transition depth. As a result, spirals of delaminated depleted material develop slowly as is observed in the F-field at 4.0 Ga.

From the decrease in the density of stream-lines in Fig. 1 with proceeding evolution it is concluded that the vigour of convection is gradually decreasing. Despite these sluggish convection rates, the compositional state of the upper mantle does show significant variations during the last 1 billion years of evolution shown.

The lateral variations of temperature in the right-hand-side column of Fig. 1 show that cold areas coincide with thick depleted continental roots. The maximum temperature is 2216°C at $t =$ 1.5 Ga and decreases to 2058°C at $t = 4.0$ Ga. Most thermal anomalies have amplitudes of ca. 300°C, and the maximum positive thermal anomaly of the shown snapshots is 616°C at $t = 2.0$ Ga.

Fig. 2 shows the evolution of several global quantities. The volume average temperature in Fig. 2a illustrates that secular cooling occurs at an almost constant rate. The drop in the volume averaged temperature due to cooling from the top is 340°C from 1740 to 1400°C.

Fig. 2b shows the evolution of the volume averaged degree of depletion $\langle F\rangle$. After the initial generation of the continental root, completed at ca. 50 Ma, three episodes follow during which the total volume of depleted material increases. The onset of these partial melting periods is marked with arrows. In spite of the overall secular cooling, upwellings apparently still cross the solidus. During the last 1.2 Ga of evolution the value of $\langle F\rangle$ remains constant because mantle differentiation has stopped after 2.8 Ga of evolution. If we assume that the initiation of continent formation in the model corresponds to 4.0 Ga b.p., the melt production stopped 1.2 Ga b.p., that is, the later Proterozoic. Several suggested continental growth curves (Windley, 1995) show a major surge of continental growth during the Mid and Late

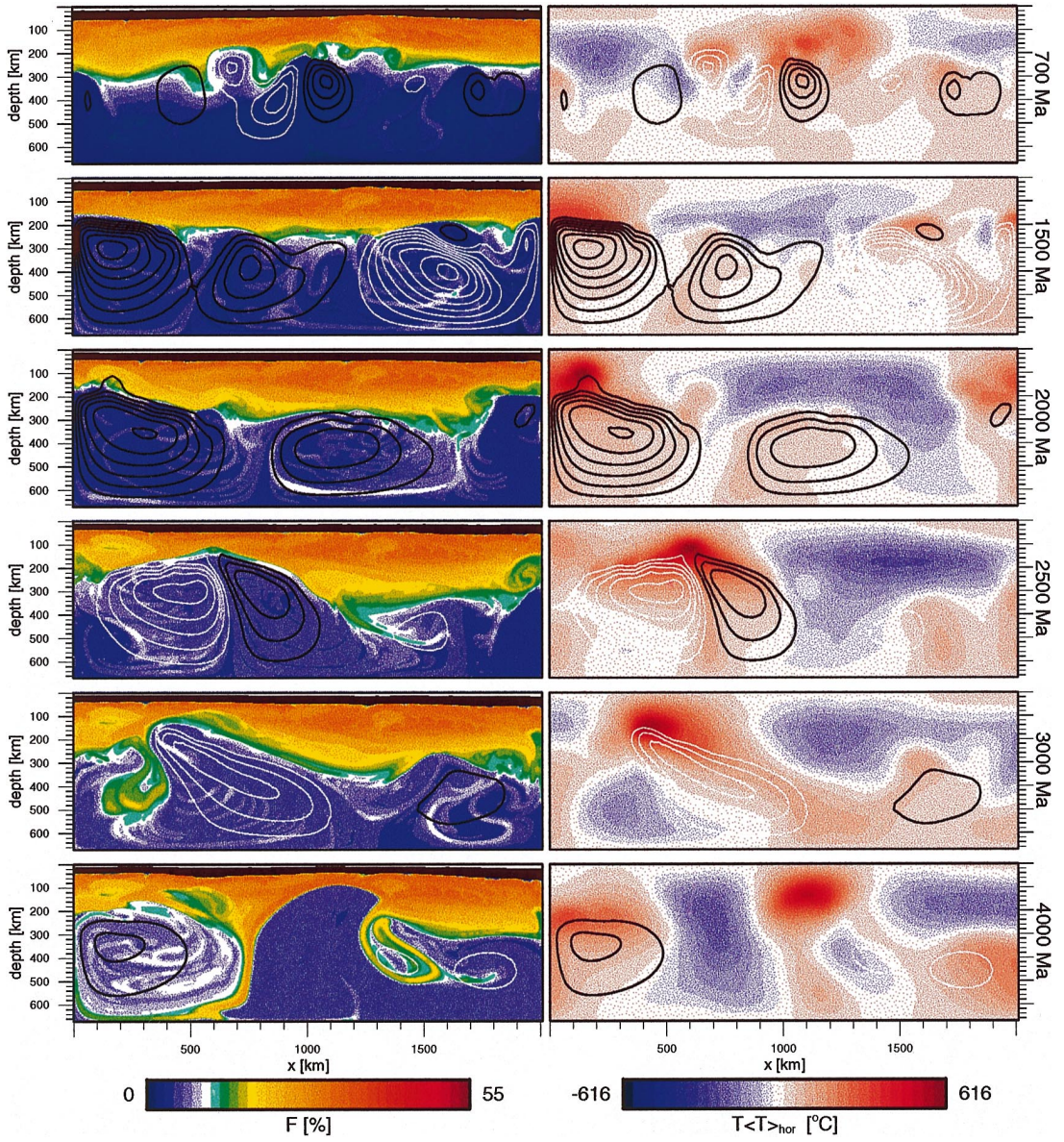

Fig. 1. The left-hand-side column shows the F-field. Evolution times are given at each frame. The white and black layers at the top are the upper and lower crustal layers, respectively. The white F-field below the crust corresponds to $9\% < F < 10\%$. The corresponding lateral variations of the temperature field (i.e., T–$\langle T \rangle_{\mathrm{hor}}$) are shown in the right-hand-side column. The black and white contour lines in all frames indicate clock and counter clockwise flows, respectively. See Section 2.1 for the time use convention.

Archaean followed by a more slowly and steadily increase in crustal volume.

Fig. 2c illustrates that convection rates slowly decrease. Besides, the amplitude of the variations in the V_{rms} decrease with time. This is caused by the progressive cooling, which results in a significant increase in the overall viscosity.

Fig. 2d shows the averaged heat flow through the Earth's surface q_0. Starting at high values of ca. $120\,\mathrm{mW\,m^{-2}}$, values decrease to ca.

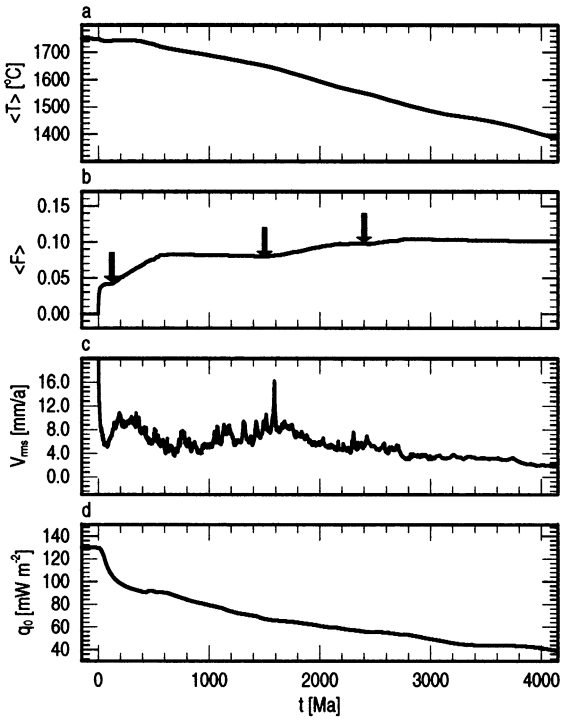

Fig. 2. Evolution of some volume averaged quantities. (a) Temperature. (b) Degree of depletion. (c) Root-mean-square velocity for which the off-scale part is shown in De Smet et al. (1998). (d) Average surface heat flow value.

40 mW m^{-2} after 4.0 Ga. Such a low surface heat flow value is reasonable for a present-day cratonic shield area (Chapman, 1986; Pollack et al., 1993). The steep decrease in q_0 during the early evolution of the model is followed by a much more steady decrease.

Fig. 2a suggests an almost constant cooling rate of the upper mantle model. On the other hand the surface heatflow decreases significantly during the 4 Ga evolution. From these curves it can be deduced that the surface heat flux is mainly produced by radiogenic heat sources, concentrated at shallow level which decrease due to radioactive decay with an effective half life time of ca. 2 Ga De Smet et al. (1999). A first order estimate of the heart flow component due to secular cooling of the upper mantle model follows from the drop in the volume averaged temperature of 340 K which represents a thermal energy decrease of $\Delta Q = 8 \times 10^{14}$ J m^{-2} in an average vertical column of unit cross section. Assuming a constant secular cooling rate in line with Fig. 2a this amounts to an average surface heatflux of 6 mW m^{-2} for the 4 Ga time window under consideration. This value corresponds well with interpretations of heat flow observations for the Canadian shield by (Jaupart et al., 1998) who report mantle heatflow contributions between 7 and 15 mW m^{-2}.

Fig. 3 shows several horizontally averaged quantities at four moments in time. Fig. 3a shows the horizontally averaged profiles for F. Due to delamination, vertical redistribution of depleted rock occurs. This results in an increase in $\langle F \rangle_{hor}$ in the 300–650 km depth range.

Fig. 3b shows the horizontally averaged temperature of the upper mantle model. Although the geotherm is below the solidus (dashed), partial melting events take place in upwellings associated with thermal anomalies that cross the solidus. After prolonged evolution, a thermal boundary layer (TBL) develops at the bottom. This is due to the thermal inertia of the heat reservoir of the lower mantle and core, and the applied impermeable lower to upper mantle transition, which buffers the cooling of the upper mantle. The decrease in temperature of the shallow model region is enhanced by the decrease in radiogenic heating, which is concentrated in the crustal layers.

Fig. 3c shows a dramatic decrease of the horizontally averaged convection rates from a maximum value of ca. 10 mma^{-1} at $t = 1.2$ Ga to 2 mma^{-1} at 4.0 Ga. Also the vertical variations in convective velocities diminish with proceeding evolution.

Fig. 3d shows the evolving viscosity profile. The strong increase in viscosity is the main cause for the decrease in V_{rms}. The decrease in averaged mantle temperature results in a less pronounced minimum viscosity in the asthenospheric layer underneath the growing MBL. The minimum value of the viscosity increases considerably by approximately two orders of magnitude from 5×10^{19} to 5×10^{21} Pas over 3 Ga. The shallow region of the continental root is stabilized by the growth of the MBL at the top. The slowly evolving TBL at the bottom causes an inversion in the deeper upper mantle viscosity profile.

Fig. 4 shows the distribution of melt produc-

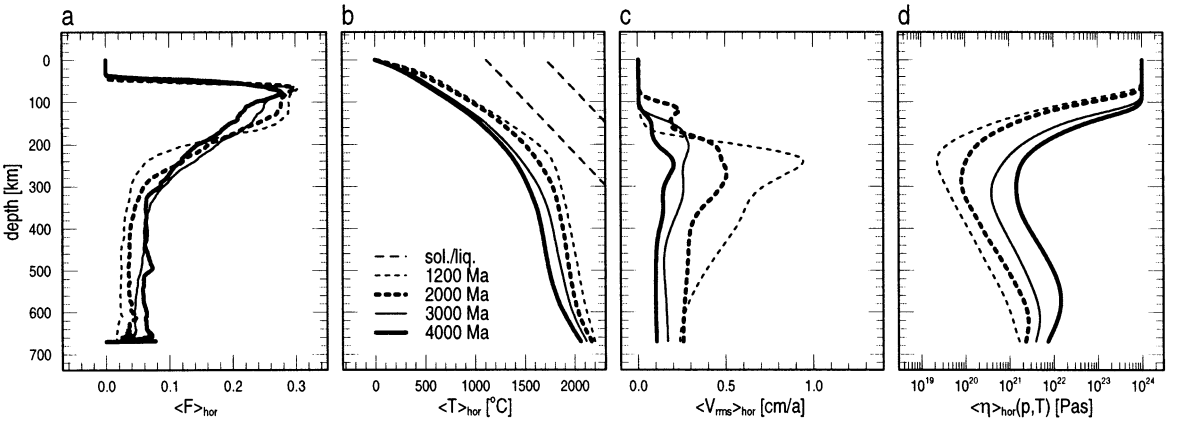

Fig. 3. Horizontally averaged profiles at several stages of the model evolution. (a) Degree of depletion. (b) Temperature. (c) Velocity root-mean-square. (d) Viscosity. The dashed curves in (b) are the solidus and liquidus equilibrium lines.

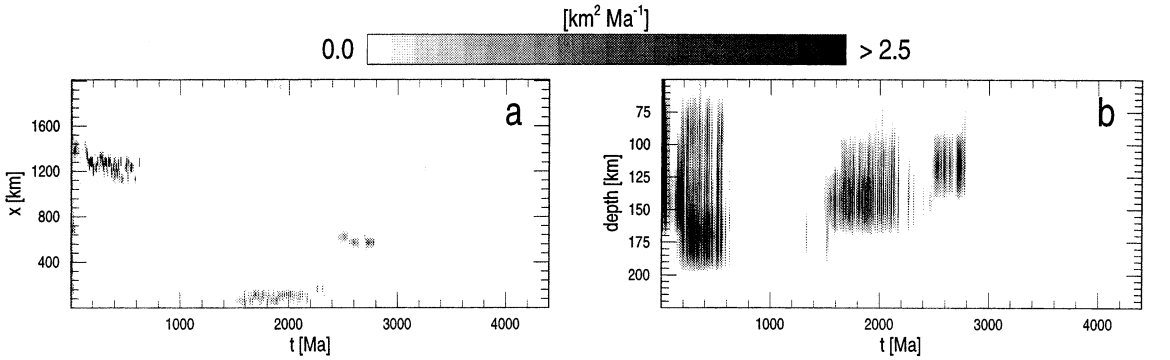

Fig. 4. The horizontal (a) and the one-dimensional depth (b) melt production distribution as a function of time. Note the three long distinct periods of partial melting (a+b), and the decrease in time of the depth range of melt production (b).

tivity versus time integrated over vertical columns (Fig. 4a) and horizontal rows (Fig. 4b). Up to 2.8 Ga three episodes of upper mantle differentiation can be recognized from 120–600 Ma, 1.5–2.2 Ga, and 2.5–2.8 Ga. Apparently, the continental upper mantle system experiences quiescent periods during which no intermittent melting occurs. During evolution the maximum depth of melting decreases [Fig. 4b] because of the decrease in mantle potential temperature with time. At the same time the growth of the MBL increases the minimum depth to which melt producing diapirs can rise.

3.2. Detailed dynamics of diapiric partial melting

In order to investigate the patterns of mantle differentiation in greater detail we applied a set of tracer particles. Each single tracer in the set tracks the histories of the degree of depletion F, the temperature T, and its position (x, z).

Fig. 5 shows several enlargements of a region where mantle differentiation occurs. The time-window from 401 to 500 Ma is part of the first period of intermittent melting events shown in Fig. 4. The positions of nine tracers are shown for eight snapshots, which are unevenly spaced in

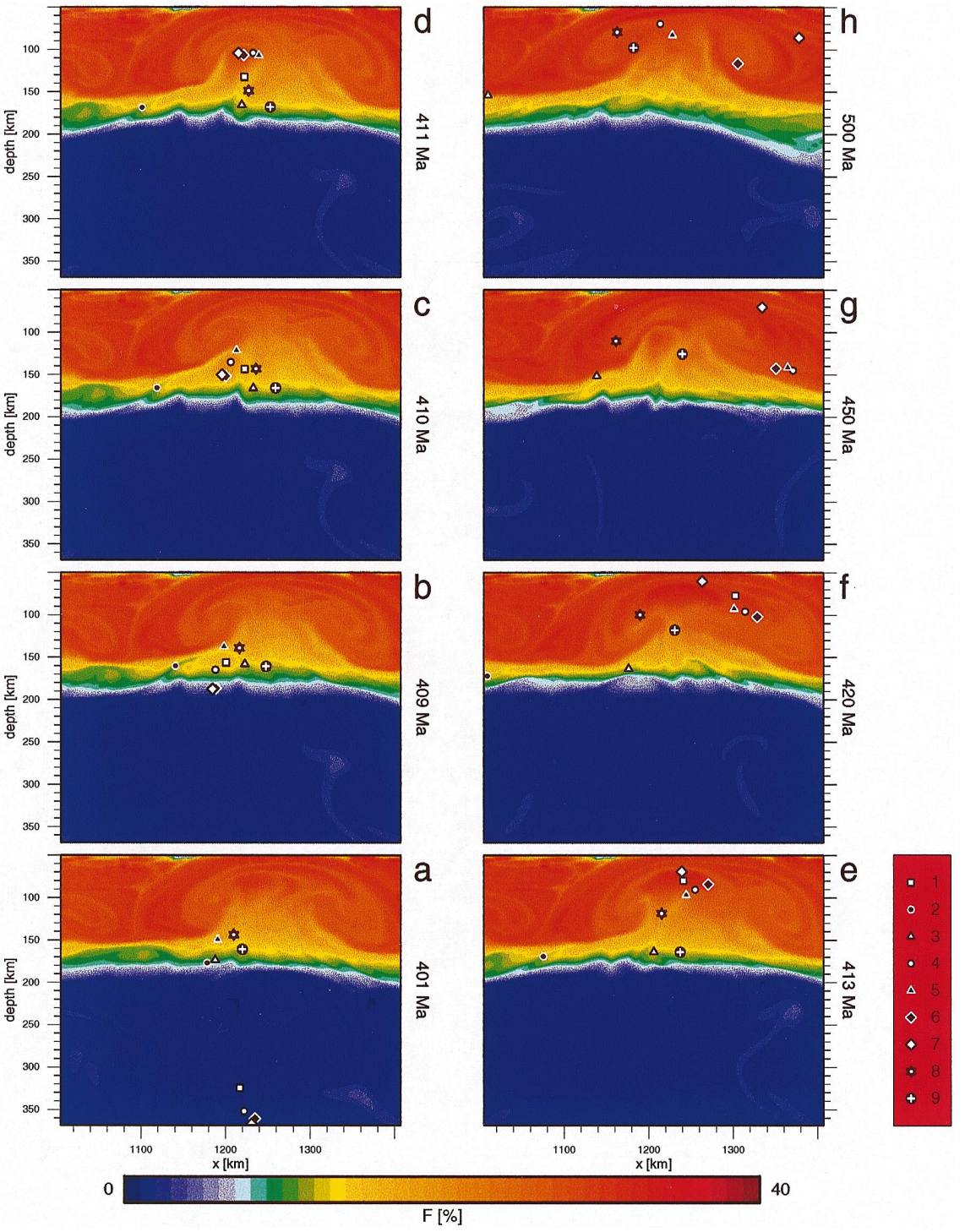

Fig. 5. Several enlargements of *F*-field snapshots illustrating the evolution of the continental root where small-scale melting diapirs impinge the depleted layer between 401 and 500 Ma. The material that melts comes from the undepleted deeper region as inferred from the flow pattern the nine tracers. This melting event corresponds to the first long period of the model evolution during which episodically melting occurs and melting starts at relatively large depths (see also Fig. 4). Note that the full available grid resolution was used in these contour plots. See Section 2.1 for the time use convention.

time. The relation between tracer symbols and corresponding numbers is given in the red legend at the bottom right-hand-side of Fig. 5.

In Fig. 5a four tracers (1, 4, 6, 7) are situated in the undepleted mantle at ca. 350 km depth at $t=401$ Ma. Following the tracer positions in time shows that they are part of a hot melt producing diapir that impinges on the continental root (Fig. 5b–h). They reach depths between 60 and 100 km and spread both laterally and vertically in the root. Their relative positions illustrate the vorticity of the mantle flow in the region where melting occurs. Furthermore, the central region of the mantle diapir, which exhibits a low F value during early ascend does not differentiate much further during the remaining ascend. This is illustrated by the F-values of tracers 1 and 4 in Fig. 5c and e.

The tracers 2 and 3 are in close proximity to each other at $t=401$ Ma (Fig. 5a) where they are part of the less depleted deeper part of the root. At $t=420$ Ma (Fig. 5f they have a much larger separation. During the time-window shown, they are mainly subject to lateral movement in the deeper part of the root where their degree of depletion is not altered.

Tracers 8 and 9 are subject to recurrent melting. Fig. 6a and b shows the (p, T, t)- and (p, F, t)-paths for tracer number 9 for the 401–500 Ma time-window. At point A the tracer has a low value of F and it slowly ascends to point B ($t=$ 413 Ma). At this point, the tracer represents a small mantle volume with $F=10\%$ which starts to rise much faster and crosses its solidus at $F=19\%$. Here, a relatively slow vertical movement around a depth of 125 km (4.2 GPa) is observed until $t=$ 450 Ma, when a further ascent to point D begins. Recurrent melting from C to D increases the degree of depletion to 26%. The uprise continues more slowly and without melting to point E after which the tracer descends to higher pressure (point F). It circulates back upward to point G, but is too cold to initiate another cycle of recurrent melting.

Three (p, T, t)-paths and corresponding (p, F, t)-paths are given in Fig. 7a and b, respectively. Each tracer is approximately situated in the centre of a melting diapir. They correspond to the

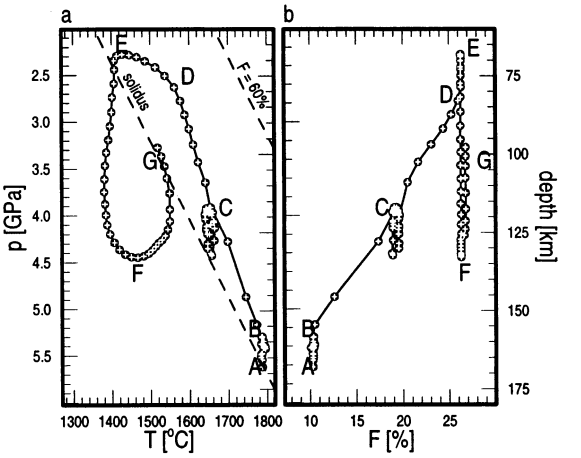

Fig. 6. (a) (p, T, t)-path for tracer that represents a mantle volume subject to recurrent melting. Time increment between symbols as indicated in the paths is 1 Ma. (b) Corresponding (p, T, t)-path. The symbols used in (a) and (b) corresponds to the tracer depicted with the same symbol in the contour plots for the F-field in Fig. 5.

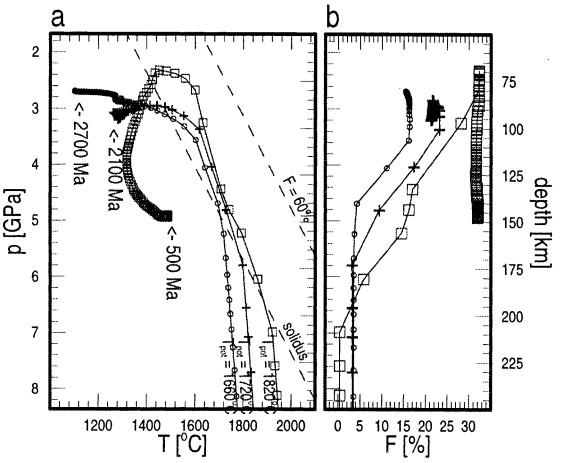

Fig. 7. (a) (p, T, t)-paths for three tracers. They correspond to tracers approximately positioned in the heart of different melt producing diapirs that impinge on the continental root. The final position of each tracer for the displayed time-window corresponds to the indicated time. Indicated times are model times (see Section 2.1). The elapsed model time between the symbols is 1 Ma. The hot and cold tracer correspond to the first and last period of melting, respectively. Tracer potential temperatures are indicated next to each (p, T, t)-path and the horizontal axis is the actual temperature. The time increment between symbols is 1 Ma. (b) (p, T, t)-paths corresponding to (a). The tracer path indicated with open squares in (a) and (b) is the tracer depicted with the same symbol in the contour plots for the F-field in Fig. 5.

three main periods of differentiation (see Fig. 4). The final position of each tracer for the displayed time-window corresponds to the indicated model time. The path marked with open squares corresponds to tracer 1 which is indicated with the same symbol in Fig. 5.

The subsolidus ascend of material occurs adiabatically and the corresponding potential temperatures T_{pot} are given in Fig. 7a. The mantle temperature decreases with time and partial melting therefore starts at shallower depth as time progresses, since the solidus is crossed at lower pressures. A hotter upwelling is capable of producing more melt over a larger depth interval and reaching higher degrees of depletion (Fig. 7b). This was also observed in the melt productivity shown in Fig. 4. When the upper mantle cools further, the MBL at the top of the mantle grows (Fig. 3d), which prevents the diapirs from penetrating the root to shallow levels. The presence of the MBL at the end of the melting path prevents further ascend after which the tracer becomes part of the stagnant layer and cools further by conductive heat loss. This is consistent with the (p, T, t)-paths derived for upper mantle samples described by Roermund and Drury (1998).

Highly depleted material is positioned directly underneath the crust during early evolution. After cooling from the top this material is trapped and can be brought to the surface during later evolution in the form of xenoliths. Bernstein et al. (1998) describes such xenoliths that contain highly depleted mantle material ($\sim$40%) originating from depths of 1–2 GPa.

After melting has stopped, the depleted material becomes part of the continental root. It maintains its attained F-value except for small effects of numerical diffusion, which causes the slow decrease in depletion observed at low pressures for the tracer path marked with crosses in Fig. 7b. This numerical diffusion is an artifact of the numerical method (De Smet et al., 2000). The two cold tracers in Fig. 7b are already modestly depleted ($F=3.5\%$) during upwelling before reaching the solidus. This is caused by the mixing of delaminated depleted material in the deeper mantle due to the finite amount of numerical diffusion, which acts as an artificial mixing mechanism in the numerical model.

3.3. Comparison with theoretical geotherms

We compare the global and local thermal state of the upper mantle model at $t=4$ Ga with theoretically derived continental geotherms for a present-day cratonic situation. The heat flow through the surface of the model has dropped to an averaged value of 41 mW m^{-2} at this point in the evolution. Surface heat flow measurements for cratonic shields with an age of >3.5 Ga range between 30 and 50 mW m^{-2} (Pollack et al., 1993). Since the model heat flow value is within this interval after 4 Ga of evolution, we compare this model state with the theoretical cratonic thermal model used by Chapman (1986) and Pollack et al. (1993). This model is thought to be valid for the relatively shallow part of the shield where conductive heat transport is dominant.

The model crustal thicknesses and heat flow values in combination with the incorporated radiogenic heat generation at $t=4$ Ga are used as the parameters for the theoretical geotherm computation as given by Chapman (1986). Note that the heat productivity in the two-dimensional convection models is based on the data also given by this author. In the model the exponential depth distribution of the heat productivity in the upper crust is simplified to an equivalent uniform value. We therefore give two theoretical geotherms: one corresponding to the exponential distribution of radiogenic heating according to Chapman (1986) and one with the equivalent uniform value. Furthermore, at large depths advective heat transport becomes more important and the theoretical geotherm deviates significantly from the results derived from the convection model.

Fig. 8a–c shows three temperature profiles derived from the convection model and Fig. 8d is the horizontally averaged state of the model. They can be compared to the corresponding theoretical geotherms defined by Chapman (1986). The thin solid lines are for an exponential distribution of radiogenic heating in the upper crust. The surface heat flow of the model are given in each frame. Lateral variations of the lower and upper crustal

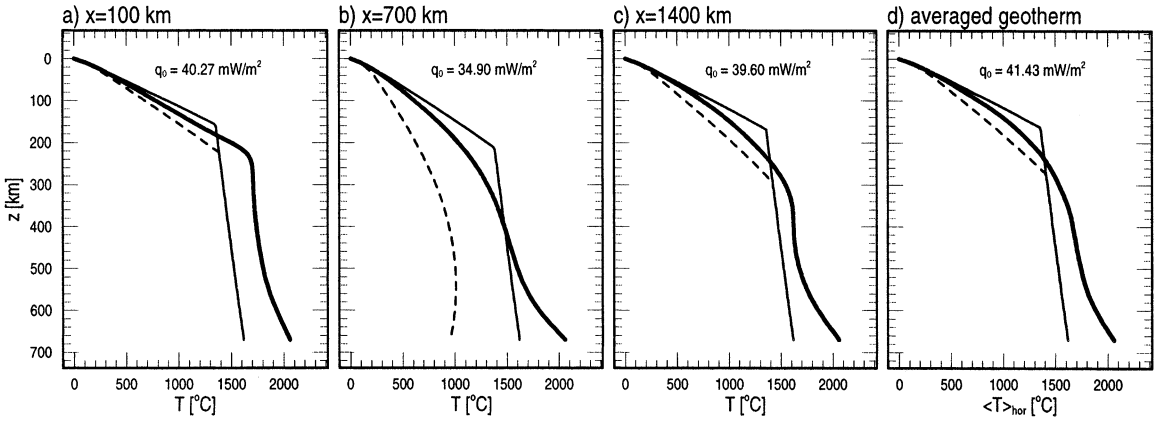

Fig. 8. (a–c) Geotherms derived from the convection model (thick solid line) at 4000 Ma at several x-locations as indicated above each frame. The last frame (d) shows the averaged temperature profile. The thin dashed and solid lines are theoretical continental geotherms as described by the model of Chapman (1986) where the heat flux at the surface (q_0) is obtained from the model. The deeper part of the theoretical curves are defined by an adiabatic geotherm corresponding to a present-day potential temperature of 1280°C (McKenzie and Bickle, 1988). The colder dashed geotherms corresponds to the uniform upper crustal radiogenic heat production at 4000 Ma as incorporated in the model. The solid thin line corresponding to an exponential distribution in the upper crust.

thicknesses in the model (see Fig. 1) are taken into account. It can be concluded from Fig. 8 that for shallow depths (<200 km) the geotherms derived from the convection model are in reasonable agreement with the continental geotherms according to Chapman (1986).

3.4. Age and compositional structure of continental roots

The mechanism of continental formation and evolution resulting from the mantle convection model presented here produces a specific structure of the continental root expressed in the thermally defined age and the composition. Samples of deep continental root material brought up as xenoliths and peridotite massifs have been used to derive information about (p, T)-conditions (Finnerty and Boyd, 1987; Boyd, 1987) age (Boyd et al., 1985; Boyd and Gurney, 1986; Pearson, 1997) and composition (Jordan, 1979; Griffin et al., 1984, 1996) of the upper mantle below continents. Here we present similar observables derived from the numerical modelling results.

The same set of tracers used in the previous section has been used to investigate the structure and evolution of the thermally defined age of the continental root. The thermal age t_{close} is defined here as the time elapsed since a rock sample cooled below a hypothetical closing temperature T_{close}. In the model calculations, the temperatures of a set of tracer particles is monitored at every time-step. When a tracer cools below the closing temperature the current model time value is stored. The closure time is reset when the closing temperature is exceeded during a later event. This thermal rejuvenation can occur by reheating during thermal events. Results are presented for several hypothetical closing temperatures ranging from 600 to 1200°C with intervals of 200°C. This is within suggested upper mantle ranges (Mezger et al., 1992). The state of the model after 4 Ga of evolution is assumed to correspond to the present-day situation, i.e., $t=4$ Ga $=0$ Ma b.p.

In the left-hand-column of Fig. 9 the evolution of the closure time is given for $T_{close}=1200$°C for snapshots starting at 2.5 Ga b.p. and ending at 0 Ga b.p. with 0.5 Ga intervals. Note that the depth-scale is twice the x-scale to emphasize the details. Deep, white areas indicate that the temperature of the material is higher than T_{close}. White upper mantle areas just underneath the crustal layers have temperatures below the T_{close} from the onset of evolution. The corresponding temperature fields are given in the right-hand-side column.

At 2.5 Ga b.p. there is a shallow feature in the

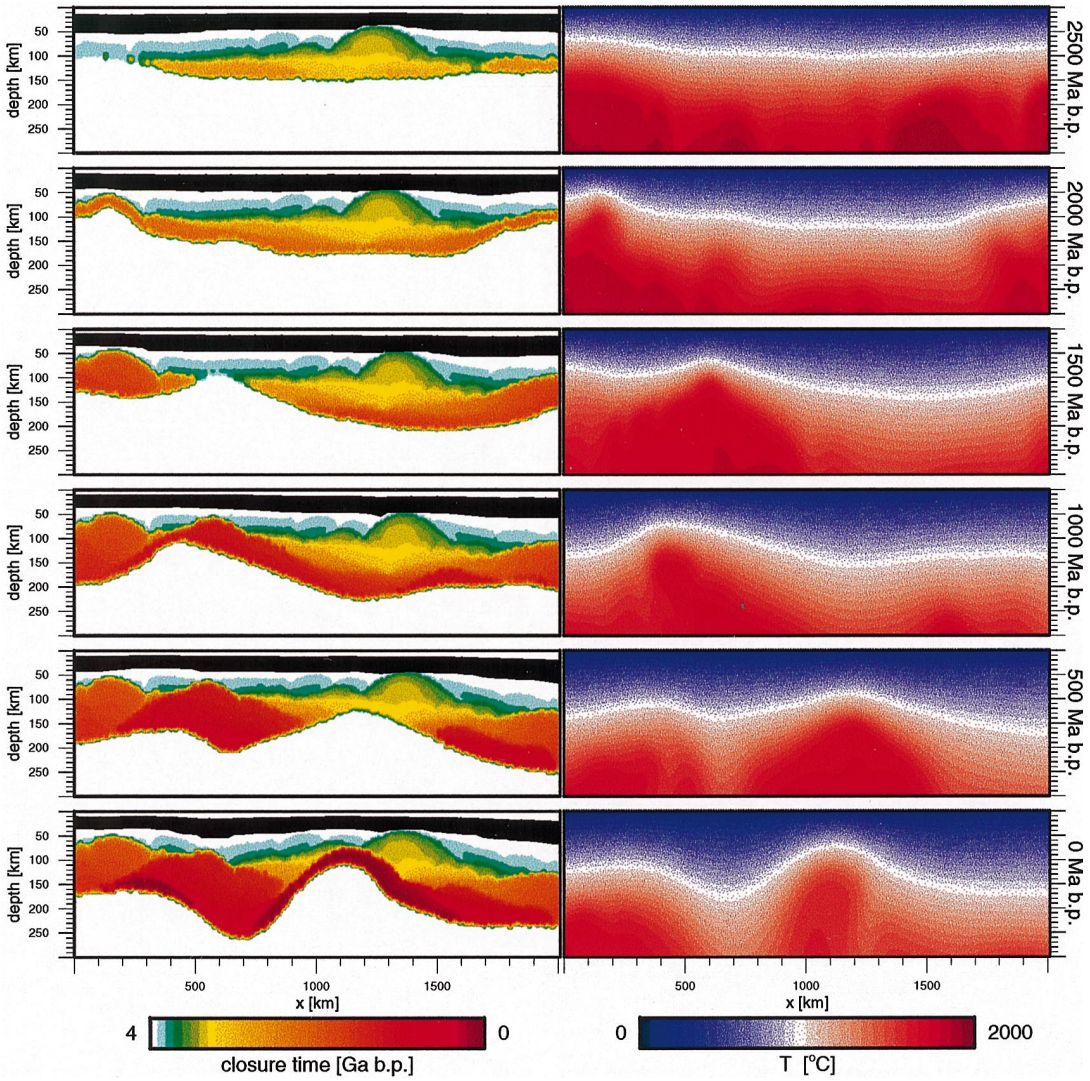

Fig. 9. Evolution of the closure time (left-hand-side column) for a closing temperature of 1200°C when 4000 Ma = 0 Ma b.p. is assumed. The white deep regions are still above the closure temperature. The transition from the coloured regions at the base to the deep, white part shows a very narrow band with old ages, which is an artifact of the post-processing and plotting procedure. This transition should be sharp from young age to no age (white). The corresponding temperature fields are depicted in the right-hand-side column. Note that the depth-scale is exaggerated twice with respect to the x-axis to emphasize the details. See Section 2.1 for the time convention use convention.

$1200 < x < 1400$ km range, which reaches the lower crust. This is the result of an older hot temperature anomaly, the remnant of a mantle diapir timed at 3.5 Ga b.p., no longer visible in the temperature field. A similar event is observed from 2.5 to 1.0 Ga b.p. at a slightly greater depth in the $100 < x < 300$ km range. The thermal anomaly that caused this feature is slowly disappearing as is illustrated by the temperature field at 2.5, 2.0 and 1.5 Ga b.p. This region on the 'left' closes within 1 Ga up to a depth of almost 200 km.

Over a depth range of $125 < z < 225$ km between $x = 1000$ and 1300 km rock reached temperatures < 1200°C at 1.0 Ga b.p. During the next 500 Ma

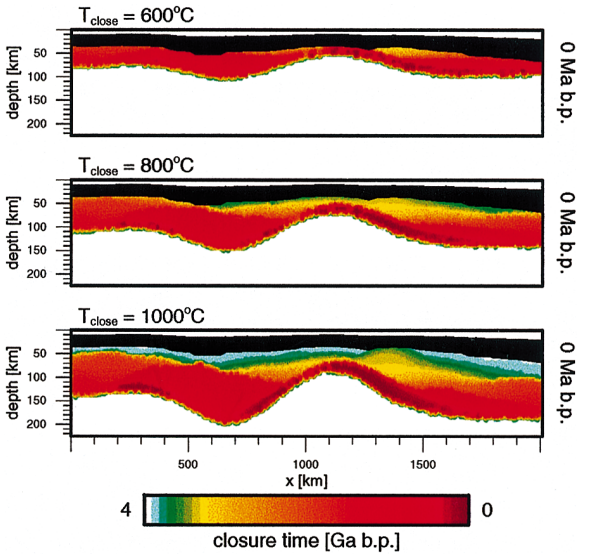

Fig. 10. The closure time fields at 0 Ma b.p. for closing temperatures of 600, 800 and 1000°C from top to bottom when 4000 Ma = 0 Ma b.p. is assumed. The depth-scale is exaggerated twice with respect to the x-axis. The white deep regions have not yet cooled enough and therefore have not sank below the closure temperature. See also the caption for Fig. 9.

of evolution, a hot upwelling resets these closure times after which the rock 'closes' again from 0.5 Ga b.p. on. A similar smaller scale process has been active between 2.0 and 1.0 Ga b.p. around $x = 600$ km.

Similar patterns are also observed for the lower range of T_{close}. Fig. 10 shows continental thermal age structures for different closing temperatures (600, 800 and 1000°C) at 0 Ma b.p. The effect of cooling from the top is reflected in the differences between the patterns of closure times at different closing temperatures.

Vertical profiles of the closure times and degree of depletion at 0 Ma b.p. are given in Fig. 11a at three horizontal positions identical to those given in Fig. 8.

Lateral variations in thermal history are illustrated by the differences between the frames in Fig. 11a1–a3. The sub-horizontal parts of these curves are the result of thermal rejuvenation, resetting the thermal age beneath the secularly growing MBL. For instance, the fast drop to greater depth of the t_{close}-curves in Fig. 11a2 at $t_{close} = 1.3$ Ga b.p. is related to the accelerated shift of the isotherms to greater depth. This thermal shift starts between 1.5 and 1.0 Ga b.p., at $x = 700$ km as shown in the temperature frames of Fig. 9.

The stratification of the compositional layering in the continental root and its lateral variation are illustrated in Fig. 11b1–b3 for the same horizontal positions as those given in Fig. 11a1–a3. The detailed structure shown in these profiles is numerically well resolved. Maximum values of $F = 30\%$ are found at shallow sub-crustal levels corresponding to the oldest depleted material in the model that was in a hot mantle during the initial phase of continental formation. This material might correspond to the strongly depleted material found in mantle xenoliths originating from shallow depths as reported by Carswell et al. (1984) and Bernstein et al. (1998). The results of partial remixing of material that delaminated from the continental root is illustrated by the low values of F in the sub-continental mantle.

4. Discussion and conclusions

The numerical modelling results show that continental upper mantle which has been formed in a relatively short period during the Archaean remains gravitationally stable for at least 4 Ga. Although small scale delamination events occur, which result in remixing of depleted continental root material in the sub-continental mantle, no large scale collapse of the continental root occurs for the observed time window. This long term stability is due to the effect of the low density of the depleted residual peridotite. This is reinforced by the effect of the temperature dependence of the viscosity which results in the growth of the strong mechanical boundary layer during secular cooling. The thickness of the resulting continental root (200–250 km) corresponds to similar values reported from seismological observations (Woodhouse and Trampert, 1995) although larger values have been reported also (Durrheim and Mooney, 1994; Polet and Anderson, 1995).

Detailed analysis of the (p, T, F, t)-paths illustrate the nature of recurrent melting in mantle diapirs which penetrate the continental root from

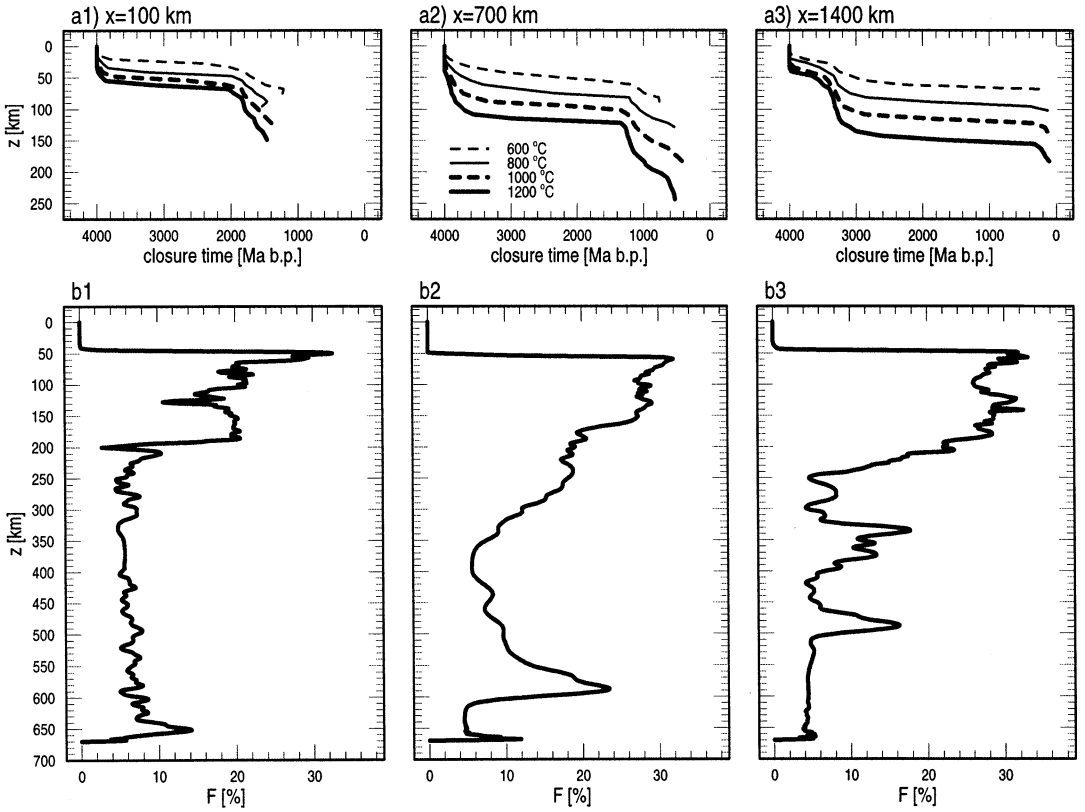

Fig. 11. Profiles of the *F*-field (b) and four closure times (a) at three *x*-locations identical to the locations used for the profiles as given in Fig. 8. The profiles correspond to $t = 4000$ Ma $= 0$ Ma b.p. for which the closure temperature fields are depicted in Figs. 9 and 10. The deeper region for which the closure time profile is not shown has temperatures higher than the indicated closing temperatures. The 'wiggles' in the *F*-profiles (b) are resolved by the numerical method.

below. The results show that partially melted material in the root can be entrained in diapiric upwellings, resulting in recurrent melting. The model (p, T, F, t)-paths show similarities with recent peridotite samples found in mantle xenoliths (Bernstein et al., 1998) and peridotite massifs (Roermund and Drury, 1998). The analysis of the thermal age of the model continental root reveals a definite layering in the thermal age with the oldest material of ca. 4 Ga situated at shallow depth directly beneath the crust. This reflects the mechanism of growth of continental lithosphere from below. Lateral variation of the thermal age increases with depth in the continental roots due to thermal rejuvenation by diapiric events in the weaker deeper parts of the root during later evolution.

Several limitations of the model should be considered. First the model configuration is limited to a completely continental upper mantle. This prevents lateral heat transport form the sub-continental mantle, which would enhance the secular cooling (Nyblade and Pollack, 1993; Pollack, 1997). At present, cratonic shields are not adjacent to oceanic upper mantle but are typically surrounded by Proterozoic continental upper mantle systems. Nevertheless, during early evolution in the Archaean those Proterozoic systems still had to be formed, and some interaction with the non-continental environment must have taken place. This requires more insight into non-continental Archaean mantle dynamics, which was probably completely different from today's situation (Vlaar et al., 1994).

An important limitation of the model is the restriction to the uppermantle domain. The lower mantle has been represented as an isothermal time dependent heat reservoir, which operates as a buffer in secular cooling. This is related to the assumption of fully layered convection, which may have prevailed especially during the earlier periods of the Earths evolution when the effective Rayleigh number for thermal convection must have been higher, thus favouring layered convection (Christensen and Yuen, 1985; Steinbach et al., 1993).

The strengthening effect of devolatilization on the rheology of the depleted mantle root has been neglected in the present model (Karato et al., 1986; Pollack, 1986; Karato and Jung, 1998). This would slow the convective cooling and increase the mechanical stability. Modelling results illustrating this effect are given by (De Smet et al., 1998).

Geotherms derived from the numerical modelling results after 4 Ga of secular cooling are in agreement with the theoretical present-day geotherms as given by (Chapman, 1986), at least for the shallow lithospheric regime, where conductive transport is dominant. Thermal evolution of the upper mantle shows a drop in average temperature of ca. 340°C and a decrease in surface heat flow from 100 to ca. 40 mW m^{-2} after 4 Ga. This is in reasonable agreement with estimates from whole mantle parameterized convection models (Jackson and Pollack, 1984).

The estimated small contribution of secular cooling of 6 mW m^{-2} to the surface heatflux compares well with the range of 7–15 mW m^{-2} given by (Jaupart et al., 1998), based on heatflow observations for the Canadian shield.

Acknowledgements

We thank Jean-Claude Mareschal and Paul Morgan for their insightful comments, which improved the manuscript. This research has been supported by the Dutch Science Foundation (NWO) and by NATO.

References

Anderson, D.L., 1990. Geophysics of the continental mantle: a historical perspective. In: Menzies, M. (Ed.), Continental Mantle. Clarendon Press, Oxford, UK, pp. 1–30.

Bernstein, S., Kelemen, P.B., Brooks, C.K., 1998. Depleted spinel harzburgite xenoliths in tertiary dykes from east Greenland: restites from high degree melting. Earth Planet. Sci. Lett. 154, 221–235.

Boyd, F.R., 1987. High- and low-temperature garnet peridotite xenoliths and their possible relation to the lithosphere-asthenosphere boundary beneath southern Africa. In: Nixon, P.H. (Ed.), Mantle Xenoliths. Wiley, pp. 403–412.

Boyd, F.R., Gurney, J.J., 1986. Diamonds and the African lithosphere. Science 232, 472–477.

Boyd, F.R., Gurney, J.J., Richardson, S.H., 1985. Evidence for a 150–200-km thick Archaean lithosphere from diamond inclusion thermobarometry. Nature 315, 387–389.

Carswell, D.A., Griffin, W.L., Kresten, P., 1984. Peridotite nodules from the Ngopetsoeu and Lipelaneng kimberlites Lesotho: a crustal or mantle origin. In: Kornprobst, J. (Ed.), Kimeberlites II: The Mantle and Crust–Mantle Relationships vol.IIB, Developments in Petrology. Elsevier Science, The Netherlands, p., 243.

Chapman, D.S., 1986. Thermal gradients in the continental crust. In: Dawson, J.B., Carswell, D.A., Hall, J., Wedepo, H.K.H. (Eds.), The Nature of the Lower Continental Crust vol. 24. Spec. Publ. Geol. Society, London, pp. 63–70.

Christensen, U.R., Yuen, D.A., 1985. Layered convection induced by phase transitions. J. Geophys. Res. 300, 10291–10300.

De Smet, J.H., Van Den Berg, A.P., Vlaar, N.J., 1998. Stability and growth of continental shields in mantle convection models including recurrent melt production. Tectonophysics 296, 15–29.

De Smet, J.H., Van Den Berg, A.P., Vlaar, N.J., 1999. The evolution of continental roots in numerical thermo-chemical mantle convection models including differentiation by partial melting. Lithos 48, 153–170.

De Smet, J.H., Van Den Berg, A.P., Vlaar, N.J., 2000. A characteristics based method for solving the transport equation and its application to the process of mantle differentiation and continental root growth. Geophys. J. Int. 140 (3), 651–659.

Doin, M.-P., Fleitout, L., McKenzie, D., 1996. Geoid anomalies and structure of continental and oceanic lithospheres. J. Geophys. Res. 101, 16119–16135.

Durrheim, R.J., Mooney, W.D., 1994. Evolution of the Precambrium lithosphere: seismological and geochemical constraints. J. Geophys. Res. 99, 15359–15374.

Ebinger, C.J., Sleep, N.H., 1998. Cenozoic magmatism throughout east africa resulting from impact of a single plume. Nature 395, 788–791.

Finnerty, A.A., Boyd, F.R., 1987. Thermobarometry for garnet peridotites: basis for the determination of thermal and compositional structure of the upper mantle. In: Nixon, P.H. (Ed.), Mantle Xenoliths. Wiley, pp. 381–402.

Griffin, W.L., Wass, S.Y., Hollis, J.D., 1984. Ultramafic xenoliths from Bullenmeri and Gnotuk Maars, Victoria, Australia: petrology of a subcontinental crust-mantle transition. J. Petrol. 25, 53–87.

Griffin, W.L., Kaminsky, F.V., Ryan, S.Y., O'Reilly, C.G., Win, T.T., Ilupin, I.P., 1996. Thermal state and composition of the lithospheric mantle beneath the Daldyn kimberlite field, YakutiaKimberlites and Structure of Cratonic Lithosphere. Tectonophysics 262, 19–33.

Jackson, M.J., Pollack, H.N., 1984. On the sensitivity of parameterized convection to the rate of decay of internal heat sources. J. Geophys. Res. 89, 10103–10108.

Jaupart, C., Mareschal, J.C., Guillou-Frottier, J., Davaille, A., 1998. Heat flow and thickness of the lithosphere in the Canadian shield. J. Geophys. Res. 103, 15269–15286.

Jordan, T.H., 1975. The continental tectosphere. Rev. Geophys. Space Phys. 13 (3), 1–12.

Jordan, T.H., 1979. Mineralogies densities and seismic velocities of garnet lherzolites and their geophysical implications. In: Boyd, F.R., Meyer, H.O.A. (Eds.), The Mantle Sample: Inclusions in Kimberlites and Other Volcanics. American Geophysical Union, Washington, DC, pp. 1–14.

Karato, S., Jung, H., 1998. Water, partial melting and the origin of the seismic low velocity and high attenuation zone in the upper mantle. Earth Planet. Sci. Lett 157, 193–207.

Karato, S., Paterson, M.S., FitzGerald, J.D., 1986. Rheology of synthetic olivine aggregates: influence of grain size and water. J. Geophys. Res. 91, 8151–8176.

LeFevre, L.V., Helmberger, D.V., 1989. Upper mantle *p* velocity structure of the Canadian shield. J. Geophys. Res. 94, 17749–17765.

Mezger, K., Essene, E.J., Halliday, A.N., 1992. Closure temperatures of the sm–nd system in metamorphic garnets. Earth Planet. Sci. Lett. 113, 397–409.

Nyblade, A.A., Pollack, H.N., 1993. A global analysis of heat flow from Precambrium terrains: implications for the thermal structure of Archaean and Proterozoic lithosphere. J. Geophys. Res. 98, 12207–12218.

Pearson, D.G., 1997. The age of continental roots. Workshop on Continental Roots. Harvard University & Massachusetts Instititute of Technology.

Polet, J., Anderson, D.L., 1995. Depth extent of cratons as inferred from tomographic studies. Geology 23 (3), 205–208.

Pollack, H., 1997. Thermal characteristics of the Archaean. In: de Wit, M.J., Ashwal, L.D. (Eds.), Greenstone Belts. Oxford University Press, Oxford, pp. 223–232.

Pollack, H.N., 1986. Cratonization and thermal evolution of the mantle. Earth Planet. Sci. Lett. 80, 175–182.

Pollack, H.N., Chapman, D.S., 1977. On the regional variation of heat flow, geotherms, and lithospheric thickness. Tectonophysics 38, 279–296.

Pollack, H.N., Hurter, S.J., Johnson, J.R., 1993. Heat flow from the Earth's interior: analysis of the global data set. Rev. Geophys. 31, 267–280.

Roermund, H.L.M., Drury, M.R., 1998. An ultra-deep ($d>200$ km) orogenic peridotite body in Western Norway. In:Fall Meeting Abstracts vol. V21E-03. AGU, p., F971.

Rudnick, R.L., McDonough, W.F., O'Connell, R.J., 1998. Thermal structure, thickness and composition of continental lithosphere. Chem. Geol. 145, 395–411.

Steinbach, V., Yuen, D.A., Zhao, W., 1993. Instabilities from phase transitions and the timescales of mantle evolution. Geophys. Res. Lett. 20, 1119–1122.

Vlaar, N.J., Van Keken, P.E., Van Den Berg, A.P., 1994. Cooling of the Earth in the Archaean, consequences of pressure-release melting in a hotter mantle. Earth Planet. Sci. Lett. 121, 1–18.

Windley, B.F., 1995. The Evolving Continents. Wiley.

Woodhouse, J.H., Trampert, J., 1995. Global upper mantle structure inferred from surface wave and body wave data. In: Fall Meeting Abstracts vol. S42C-9. AGU, p., F422.